AD-A151 496 AN EXPERIMENTAL TECHNIQUE FOR THE STUDY OF VELOCITY PROFILES IN A LAMINAR JET USING A PULSED NITROGEN LASER (U) NAVAL POSTGRADUATE SCHOOL MONTEREY CA 1/1

UNCLASSIFIED D T ARMSTRONG SEP 84 F/G 20/4 NL

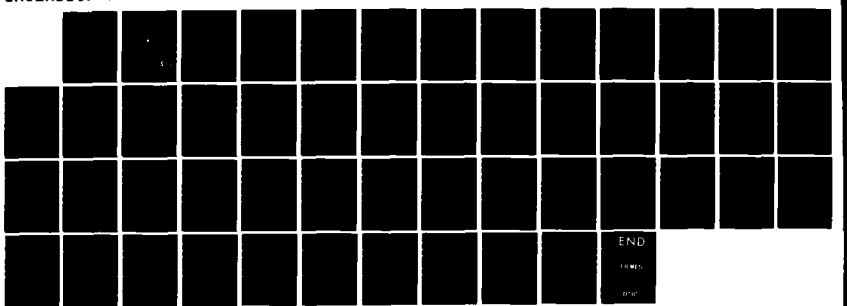

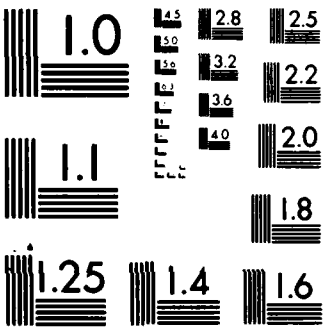

NAVAL POSTGRADUATE SCHOOL
Monterey, California

THESIS

AN EXPERIMENTAL TECHNIQUE FOR THE STUDY OF VELOCITY PROFILES IN A LAMINAR JET USING A PULSED NITROGEN LASER

by

David Thomas Armstrong

September 1984

Thesis Advisor: W. G. Culbreth

Approved for public release; distribution unlimited.

UNCLASSIFIED

SECURITY CLASSIFICATION OF THIS PAGE (When Data Entered)

REPORT DOCUMENTATION PAGE	READ INSTRUCTIONS BEFORE COMPLETING FORM
1. REPORT NUMBER	2. GOVT ACCESSION NO. A151496 / 3. RECIPIENT'S CATALOG NUMBER
4. TITLE (and Subtitle) An Experimental Technique for the Study of Velocity Profiles in a Laminar Jet Using a Pulsed Nitrogen Laser	5. TYPE OF REPORT & PERIOD COVERED Master's Thesis; September 1984
	6. PERFORMING ORG. REPORT NUMBER
7. AUTHOR(s) David Thomas Armstrong	8. CONTRACT OR GRANT NUMBER(s)
9. PERFORMING ORGANIZATION NAME AND ADDRESS Naval Postgraduate School Monterey, California 93943	10. PROGRAM ELEMENT, PROJECT, TASK AREA & WORK UNIT NUMBERS
11. CONTROLLING OFFICE NAME AND ADDRESS Naval Postgraduate School Monterey, California 93943	12. REPORT DATE September 1984
	13. NUMBER OF PAGES 49
14. MONITORING AGENCY NAME & ADDRESS(if different from Controlling Office)	15. SECURITY CLASS. (of this report) Unclassified
	15a. DECLASSIFICATION/DOWNGRADING SCHEDULE

16. DISTRIBUTION STATEMENT (of this Report)

Approved for public release; distribution unlimited.

17. DISTRIBUTION STATEMENT (of the abstract entered in Block 20, if different from Report)

18. SUPPLEMENTARY NOTES

19. KEY WORDS (Continue on reverse side if necessary and identify by block number)

Laser Velocimetry, Fluid Velocity Profiles, Flow Visualization Techniques

20. ABSTRACT (Continue on reverse side if necessary and identify by block number)

A nonintrusive technique for flow visualization of momentum jets has been investigated. A flow system containing a fluid photosensitive to ultraviolet radiation (a solution of mineral spirits and photochromic dye) has been constructed for generating a momentum jet in a test chamber. An ultraviolet beam (337.1 nm)

DD FORM 1 JAN 73 1473 EDITION OF 1 NOV 65 IS OBSOLETE

S/N 0102-LF-014-6601

UNCLASSIFIED

SECURITY CLASSIFICATION OF THIS PAGE (When Data Entered)

from a pulsed nitrogen gas laser was fired through the test chamber producing opaque traces in the jet and ambient fluid. Movement of the fluid deformed these traces and produced a record of fluid flow. Velocity distributions have been obtained in laminar jets.

Fluid velocity profiles and Flow visualization

Approved for public release; distribution unlimited.

An Experimental Technique for the Study of Velocity Profiles in a Laminar Jet Using a Pulsed Nitrogen Laser

by

David T. Armstrong
Lieutenant Commander, United States Navy
B.S.E.E., Purdue University, 1975

Submitted in partial fulfillment of the
requirements for the degree of

MASTER OF SCIENCE IN MECHANICAL ENGINEERING

from the

NAVAL POSTGRADUATE SCHOOL
September 1984

Author: 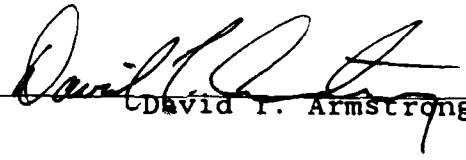
David T. Armstrong

Approved by: 
William G. Culbreth, Thesis Advisor


Paul J. Marto, Chairman,
Department of Mechanical Engineering


John N. Dyer,
Dean of Science and Engineering

ABSTRACT

A nonintrusive technique for flow visualization of momentum jets has been investigated. A flow system containing a fluid photosensitive to ultraviolet radiation (a solution of mineral spirits and photochromic dye) has been constructed for generating a momentum jet in a test chamber. An ultraviolet beam (337.1 nm) from a pulsed nitrogen gas laser was fired through the test chamber producing opaque traces in the jet and ambient fluid. Movement of the fluid deformed these traces and produced a record of fluid flow. Velocity distributions have been obtained in laminar jets.

TABLE OF CONTENTS

LIST OF TABLES

LIST OF FIGURES

I. INTRODUCTION

A variety of techniques have been developed for the visualization or measurement of velocity profiles in flowing fluids. These techniques can be generally divided into intrusive and non-intrusive categories. Among the intrusive techniques are the use of aluminum flakes to demonstrate surface flows in liquids, laser Doppler velocimetry, tell-tale streamers, hot-wire anemometers, the introduction of gas bubbles into flowing liquids, and pressure probes. The inherent problem with the intrusive methods is the error resulting from the solid particles used as tracer materials not accurately following flow streamlines or the disturbance of the fluid flow caused by the introduction of a sensor. Non-intrusive techniques such as smoke or dye traces, shadowgraphs, schlierens, and interferometers eliminate this problem to some extent, although determination of velocity profiles are difficult.

The techniques employed in this work were non-intrusive yet allowed the determination of velocity profiles because, unlike most non-intrusive methods, the trace was introduced across the flow instead of along streamlines. The tracer used was a photochromic spiropyran dye that, when dissolved in a hydrocarbon solvent, produced a rapid color change from transparent to violet upon exposure to ultraviolet light. A pulsed nitrogen laser, the source of ultraviolet radiation, was repeatedly fired through the photosensitive fluid and produced the violet traces along the laser beam path. The traces were deformed by subsequent motion of the fluid and provided a time history of the hydrodynamics.

In this work, the photochromic dye technique was employed to study velocity profiles in laminar jets. A flow

system was constructed for generating laminar jets in a test chamber. A previously constructed pulsed nitrogen laser [Ref. 1] was modified to increase the output. Data analysis was conducted by photographing the flow, digitizing the position of the traces, measuring the time interval between the laser firings, and computing the local velocity distribution in the flow for a variety of flowrates.

II. PREVIOUS WORK

The use of a photochromic dye for the study of velocity profiles was first attempted in 1962 by Miller with little success [Ref. 2]. In 1965, Goldfish, Koutsky, and Adler [Ref. 3] exposed a photochromic solution flowing through a clear glass section to the light of a xenon flash tube. A bulk tracer 1 inch long and 3/8 inch in diameter was produced and followed by a colorimeter. It was suggested that the method could be used for observing velocity profiles, boundary layers and other flow phenomena, although details of this application were not provided. Popovich and Hummel developed the technique of flash photolysis in 1966 [Ref. 4]. Using a .1% by weight solution of 2(2,4-dinitro benzyl)-pyridine (DNBP) in 95% ethanol, they produced a blue tracer line in a test section to study the viscous sub-layer in turbulent pipe flow. The pyridine dye became blue in less than 3 microseconds after exposure to high intensity light and reverted to its transparent form several milliseconds after the formation of the trace. The resulting deformation of the traces was analyzed to give the velocities in the laminar sublayer and in the buffer layer. Results were compared with Reichardt's and Diesler's velocity curves and showed good agreement [Ref. 1: p.12].

The use of photochromic dye exposed to high energy fluxes of ultraviolet light is not always a non-intrusive technique. In work conducted by Humphrey, et al [Ref. 5], violent disturbances were produced in a pendant droplet of chlorobenzene containing photochromic dye when exposed to the beam of a high power pulsed ruby laser. These disturbances were attributed to the formation of tiny gas bubbles in the fluid along the path of the laser beam [Ref. 1: p.12].

Humphrey, Hummel, and Smith [Ref. 6] conducted flow visualization studies of growing droplets of solvents in an immiscible ambient fluid. Their technique employed a commercial multipulse nitrogen laser in place of the xenon flash tube for exposing the photochromic dye. Equations were provided for correcting trace positions induced by the optical refraction between the two fluids and for subsequent computation of velocity profiles in the droplet from the corrected trace positions.

A custom built pulsed nitrogen laser and photochromic dye were employed by Culbreth, Johnson, and Marschall [Ref. 7] to study droplets of mineral spirits rising in water as part of a study of direct-contact heat transfer. The pulsed laser-produced traces within the droplet were photographed by a high speed movie camera operating at 400 frames per second and provided a film history of the deformation of the traces. Pellin [Ref. 1] conducted a study of velocity profiles in a growing droplet using a pulsed nitrogen laser of the same design. Still photographs were obtained of a growing droplet containing several traces equally spaced in time. A computer code was provided for calculating the refraction corrected position of the traces and for computing the velocity profile within the droplet.

The same laser design used by Culbreth, et al [Ref. 7] and Pellin [Ref. 1] was used in the present work and consisted of a high voltage power supply, a source of nitrogen gas, a vacuum pump, the laser channel and capacitor assembly, and associated electronics [Ref. 1 p. 13]. This simple, inexpensive, and powerful laser was designed by James G. Small and reported in [Ref. 8]. Details of the laser constructed for the present study are discussed later.

The history of the photochromic dye flow visualization technique has been described. The method was non-intrusive and afforded both flow visualization and relative ease in

determination of velocity profiles for a variety of fluid dynamics studies. The facility used by Pellin here at NPS has been modified for this work. Velocity distributions have been obtained in laminar jets and the necessary computer codes for digitizing and reducing data are presented.

III. EXPERIMENTAL APPARATUS

A. GENERAL

The apparatus shown in figure 1 consists of the fluid flow system and the optical system. The purpose of the flow system was to generate a steady, vertical laminar jet of photochromic fluid in the test chamber at a variety of flow rates. The purpose of the optical system was to expose the jet to pulsed, high intensity ultraviolet radiation at timed intervals and to photograph the resulting traces produced in the jet.

B. FLOW SYSTEM

The flow system (figure 2) consisted of the photochromic fluid, test chamber, head tank, fluid reservoir, pump, flowmeter, throttling valve, bypass valve, and connecting tubing. All components were thoroughly cleaned during assembly to minimize system contamination. Fluid from the reservoir was pumped by a variable speed, positive displacement pump to the head tank approximately 1.5 meters above the reservoir. Head tank fluid level was maintained at a constant level by a drain tube which returned excess pump flow to the reservoir. Fluid flowed from the bottom of the head tank through the flowmeter and throttling valve into the jet nozzle mounted in the bottom of the test tank. Fluid from the test chamber overflowed through three drainage ports located at the top of the chamber and was returned to the reservoir. In order to facilitate the purging of air from the system, a bypass valve was installed to shunt flow around the flowmeter and throttling valve. This provided flow rates well above the maximum permitted by the flowmeter.

1. Photochromic Fluid

The photochromic fluid used was a 50 ppm solution of 1,3,3-triethylindoline-6'-nitro-benzospirospyran (TNBSP) dissolved in mineral spirits. TNBSP is less toxic than the DNBP dye discussed previously, but is still easily dissolved in organic solvents and responds to ultraviolet light in approximately the same manner. TNBSP undergoes a color shift from transparent to violet in less than 5 microseconds and reverts to the colorless state in several seconds. Dye concentration was determined by preliminary experiments in which the nitrogen laser was fired into a container of photochromic solution and the length of the resulting trace was measured. In consideration of the jet nozzle geometry within the test chamber, a 2.5 cm trace was desired in order to completely penetrate the jet. Initial testing with a 345 ppm solution yielded trace penetration on the order of 3 mm. Subsequent testing down to 22 ppm provided traces greater than 3 cm long but these traces were very faint and it was speculated that they would be diffused rapidly when jet flow was established. The 50 ppm solution resulted in traces with the minimum 2.5 cm length. Qualitatively, these traces were well-defined and were expected to persist sufficiently when undergoing the deformation of the flowing environment.

2. Test Chamber

The test chamber shown in figures 1 and 2 was constructed of plexiglas with the exception of the front wall through which the laser beam passed. This wall was constructed of thin (approximately 3 mm) plate glass in order to minimize attenuation of the ultraviolet beam. Three possible nozzle locations were provided in the base of the test chamber. For this work, a 0.794 mm (0.03125 in) diameter nozzle was installed in the location closest to the

front wall. The test chamber was mounted on a laboratory scissors jack in order to change the vertical position of the jet exposed to the laser beam. Bubble levels were installed on the base of the test chamber to ensure vertical alignment of the chamber.

C. OPTICAL SYSTEM

The optical system (figure 1) consisted of the pulsed nitrogen gas laser, a 12 cm focal length lens, a strip chart recorder, a tungsten lamp, reflective background, and a 35 mm single lens reflex camera. The pulsed nitrogen laser provided the ultraviolet light which was focused by the lens into a fine beam passing horizontally through the jet in the test chamber. The camera, lamp, and reflective background were used to illuminate and photograph the dye traces produced in the jet. Signals from the camera and the nitrogen laser were inputted to the strip chart to provide a time record of the laser firings and camera shutter operation.

1. Pulsed Nitrogen Gas Laser

The basic principle of nitrogen gas laser operation is to excite as many molecules as possible in a very short period of time (10 nanoseconds). For this laser design, this is accomplished by creating a high voltage discharge in the laser channel, a rectangular plexiglas enclosure contained flowing nitrogen gas at 26-28 in Hg of vacuum. The upper plates of two external capacitors led into the laser channel forming a pair of parallel electrodes within the channel. The two upper capacitor plates shared a common lower (ground) plate which extended on either side of the channel. Figure 3 shows how these capacitors developed the rapid, high voltage discharge. The capacitors were charged

by the high voltage power supply providing current to one upper plate, through an inductor connected across the laser channel electrodes, to the second upper plate. The discharge of a spark gap between the second upper plate and the ground plate created a high velocity, zero-potential circular boundary which traversed the second capacitor toward the laser channel. When this zero-potential front reached the electrode in the laser channel, a very high potential difference was created between that electrode and the charged electrode of the first capacitor. For this size apparatus, the potential difference occurred across the length of the laser channel electrodes in less than .2 nano-seconds. The inductor across the laser channel electrodes opposed a rapid change in current and thus acted like an open circuit to the capacitor discharge. This permitted a high voltage discharge across the laser channel electrodes. Free electrons in this discharge collided with electrons in the nitrogen molecules and elevated them to the upper laser level (figure 4). When the electron relaxed to the lower laser level, a photon was emitted at 337.1 nm wavelength. Laser action was created by this photon interacting with other nitrogen molecules to emit identical photons. The laser action was rapidly terminated in nitrogen when the photons encountered more absorbing molecules than excited molecules. This usually occurred within 10 ns. The overall result was a very powerful, short duration pulse of ultra-violet radiation. For this laser, peak power was 200-300 megawatts with a pulse duration of approximately 9 ns.

The pulsed nitrogen laser used in this work was a modification of the same laser used by Pellin [Ref. 1] and a detailed description of the laser's construction was provided in that reference. Figure 5 shows the laser system consisted of the laser channel, capacitors, spark gap, nitrogen gas supply, vacuum pump, and high voltage power

supply. Nitrogen gas was supplied by a high pressure nitrogen flask to the front of the laser channel through a pressure regulator and cutout valve. The vacuum pump and a 0-30 in Hg vacuum gauge were connected to the rear of the channel. The pressure regulator was used to reduce flask pressure to 10 PSI at the cutout valve. With the vacuum pump operating, the cutout valve was adjusted to provide the 26-28 in Hg vacuum pressure within the laser channel. The modifications to Pellin's laser consisted of the installation of a spark gap in lieu of the thyratron and triggering circuit and several safety modifications. The spark gap functioned as an extremely fast switch for high voltage energy as follows. When the voltage potential across the air gap separating the two electrodes of the spark gap reached the breakdown voltage of the air, electrons passed through the air gap creating a path of ionized air and, therefore, depleted the charge between the laser capacitor plates. As the potential between the electrodes decreased during discharge, the resistance of the ionized air in the spark gap promptly shut off the flow of electrons and allowed the capacitor plates to recharge. The spark gap was installed with the intention of simplifying laser operation and improving output power by reducing capacitor discharge time. Laser firing rate was determined by the length of the spark gap and the voltage of the power supply. Optimum laser performance was achieved with a spark gap of approximately 1 cm. Pulse repetition rate ranged from .5 Hz at 16 KV to 4 Hz at 30 KV. A plexiglas enclosure was constructed to contain the laser channel and capacitor assembly. This enclosure attenuated stray ultraviolet light generated by the laser channel and the spark gap and reduced the shock hazard associated with laser operation. A 2 inch square hole was cut in the enclosure at the beam exit to prevent attenuation by the plexiglas. A shorting probe was

installed to facilitate discharging the laser capacitors after use and when making adjustments to the spark gap. In order to comply with the Class IV laser requirements of the American National Standards Institute (ANSI) for the safe use of lasers [Ref. 9], a key-lock switch was installed on the laser power supply and interlocks were installed on the laser enclosure and the laser laboratory door. These interlocks disabled the power supply if the laser cover was not securely in place or if the door was not closed. It is emphasized that although quite simple in construction and operation, this laser has the highest (most hazardous) ANSI laser classification due to its operating wavelength and output power. This necessitated strict adherence to safety precautions, most importantly the use of approved attenuating goggles and observing proper operating procedures.

2. Photographic Apparatus

The photographic apparatus consisted of the camera, a tungsten lamp, and a reflective background. The camera used was a Nikon F-3 HP with a Micro-NIKKOR 55 mm 1:2.8 lens mounted on the combined set of extension tubes K-1, K-2, K-3, K-4, and K-5. This combination provided a macrophotograph with an image-to-subject ratio of 1.25:1. Depth of field was very shallow with this configuration although not critical since the traces were also very narrow and contained in the vertical plane. The camera body was mounted vertically on a tripod in order to photograph the greatest vertical range of the jet. Lighting was provided by a ColorTran Multi-6 650 watt, 3200 K tungsten lamp mounted behind and above the camera. A white reflective background was installed on the opposite side of the test chamber to improve illumination and contrast. A variety of films were tried as the photographic technique was developed. The best results were obtained with Kodachrome 40A.

Although slow in speed (ASA 40), this film produced the highest resolution. Because slide transparencies were to be utilized for data reduction, black-and-white film was not used due to its limited availability in this form.

3. Event Recorder

A Gould Brush 280 dual channel strip chart recorder was used to record the timing interval of laser firings and camera shutter release. A single channel was used to record both events. The camera's flash synchronization switch was wired in series with the calibration source of the strip chart recorder and connected to the input terminals of the recorder to provide a 1 volt negative pulse when the camera shutter was released. Laser firing input was obtained by connecting one end of a 6 foot insulated wire to the ungrounded terminal of the recorder input. This wire served as an antenna which detected the RF energy pulse coincident with the discharge in the laser channel and subsequent recharging of the capacitors by the power supply. The strip chart recorded the laser firings as individual, high speed sawtooth waveforms.

IV. EXPERIMENTAL PROCEDURE

A. FLOW SYSTEM OPERATION

Flow was initiated by first filling the head tank with fluid pumped from the reservoir. Pump speed was then reduced to the minimum required to provide continuous return flow from the head tank to the reservoir. Use of the flowmeter bypass valve was necessary only for the initial flow system operation in order to facilitate the purging of air from the tubing. Jet flow was established by adjusting the needle valve built into the rotameter for the desired flow rate. The photosensitive fluid was recirculated through the system until equilibrium temperature was achieved.

B. PULSED NITROGEN LASER OPERATION

Again referring to Figure 5, laser operation was initiated by operating the vacuum pump to evacuate air from the laser channel. With the cutout valve closed, the nitrogen flask valve was opened to charge the pressure regulator. The regulator was set to 10 PSI and the cutout valve was slowly opened to supply nitrogen to the laser channel. The cutout valve was adjusted to give a 27.3 in Hg reading on the vacuum gauge. This pressure was found to provide optimum laser performance. Prior to energizing the high voltage power supply, the spark gap electrodes were cleaned by filing lightly and the gap adjusted to approximately 1 cm. Clean electrode surfaces were essential to good laser performance, possibly because the resistance of corrosion products on these surfaces retarded the capacitor discharge time. At this point, safety precautions dictated that all personnel in the laser laboratory don approved attenuating

goggles. With the laser cover securely in place and the laser laboratory door closed, the high voltage power supply was energized. As the output voltage was increased, it was found that observing output current was useful in determining the condition of the capacitor dielectric (mylar film). At 15 KV an output current in excess of 100 microamps usually indicated breakdown of the dielectric requiring replacement of the mylar sheets. With acceptable current readings, voltage was increased to give the desired laser firing rate. The laser beam was then focused by adjusting the sliding lens mount to obtain the sharpest traces in the test chamber. The scissors jack was used to elevate the test chamber until the laser beam was firing just above the jet nozzle. The horizontal position of the test chamber was then adjusted to ensure the laser beam passed directly through the center of the jet.

C. PHOTOGRAPHY

Optical alignment of the camera was accomplished by extending the lens until the circumference of the lens guard was flush against the side wall of the test chamber and the jet nozzle was centered in the viewfinder. This ensured that the axis of the camera was perpendicular to the wall of the test chamber. With alignment complete, the lens was then adjusted for proper focus. After turning on the tungsten lamp, the aperature and shutter speed were set using the internal exposure meter of the camera. The best results were obtained with Kodachrome 40A (ASA40) film at f2.8 and f4.0 with a shutter speed of 1/125 sec. While observing the traces in the viewfinder, the power supply voltage was adjusted to provide at least four clear traces. The strip chart recorder was energized several seconds prior to releasing the shutter in order to record the laser trace

intervals and shutter operation. After each photograph, the high voltage power supply was reduced below that required for laser operation. A 10-15 second waiting period permitted sufficient time for the exposed dye in the stagnant fluid adjacent to the front wall to revert to its transparent state. This procedure was necessary to reduce beam attenuation caused by dye saturation in this region.

V. DATA ANALYSIS

A. DATA REDUCTION

Data reduction was performed by projecting the slide transparencies onto a fine grid graph paper and outlining the traces on the paper. The outside diameter of the nozzle was also marked on the paper to reference trace positions and to provide a scale for the enlargement of projection. Four photographs showing at least four traces each were digitized in this manner over a range of approximately five nozzle diameters. A Cartesian coordinate system was used with the origin positioned at the center of the jet nozzle exit. The Y-axis was vertical and positive in the direction of flow. The X-axis was horizontal and positive in the direction towards the laser. The digitized positions were multiplied by the ratio of the actual nozzle diameter (0.794 mm) to the projected nozzle diameter to give X and Y values corresponding to the distance in millimeters from the origin.

B. VELOCITY DETERMINATION

Each of the four traces were curve fitted using a fourth order polynomial curve fit i.e.,

$$F(x) = a(I) + b(I)x + c(I)x^2 + d(I)x^3 + e(I)x^4 \qquad (5.1)$$

where a(I), b(I), c(I), d(I), and e(I) were time dependent and were calculated by a least squares fit of equation 5.1 to the experimental values of x and y.

Although a circular jet was generated, symmetry was assumed about the Y-Z plane only due to uncertainty about

the effects of the front wall on jet flow. The jet nozzle was located 90 mm from the wall in the negative x-direction but only 8 mm from the glass wall used to allow entrance of the laser beam in the positive x-direction. Velocity profiles were determined by following the change in position of an element of fluid over an increment of time. Figure 6 shows three typical jet traces occurring at equal time intervals (ΔT). The incremental volume of fluid contained between traces 1 and 2 (Va) was distorted to an equivalent volume (Vb) conforming to the shape given by traces 2 and 3 at a time ΔT later due to the flow field. Using the midpoints of the peripheral boundary of this element as it moves between successive traces, and assuming the volume is small, the velocity vector was approximated by:

$$\bar{V} = \overline{AB}/\Delta T \tag{5.2}$$

Given traces 1 and 2,

Let Ax = X coordinate of point A
Let Bx = X coordinate of point B

Then,

$$\begin{aligned} Ay = {} & 1/2[a(2)-a(1) + (b(2)-b(1))Ax \\ & + (c(2)-c(1))Ax^2 + (d(2)-d(1))Ax^3 \\ & + (e(2)-e(1))Ax^4] + F(Ax) \end{aligned} \tag{5.3}$$

and the volume of the element was given by,

$$\begin{aligned} Va = {} & 2\pi\int[a(2)-a(1) + (b(2)-b(1))x \\ & + (c(2)-c(1))x^2 + (d(2)-d(1))x^3 \\ & + (e(2)-e(1))x^4] \; x \; dx \end{aligned} \tag{5.4}$$

Performing the integration,

$$Va = (a(2)-a(1))Ax^2/2 + (b(2)-b(1))Ax^3/3 + (c(2)-c(1))Ax^4/4 + (d(2)-d(1))Ax^5/5 + (e(2)-e(1))Ax^6/6 \quad (5.5)$$

Given traces 2 and 3,

Let Bx = X coordinate of point B
Let By = Y coordinate of point B

In the same manner that equation 5.4 gave Va, the volume contained by traces 2 and 3 was given by,

$$Vb = (a(3)-a(2))Bx^2/2 + (b(3)-b(2))Bx^3/3 + (c(3)-c(2))Bx^4/4 + (d(3)-d(2))Bx^5/5 + (e(3)-e(2))Bx^6/6 \quad (5.6)$$

Since Va = Vb, equation 5.6 was solved for Bx. Substituting this value into the following equation gave By:

$$By = 1/2[a(3)-a(2) + (b(3)-b(2))Bx + (c(3)-c(2))Bx^2 + (d(3)-d(2))Bx^3 + (e(3)-e(2))Bx^4] + F(Bx) \quad (5.7)$$

The velocity was then given by:

$$V = \sqrt{(Bx-Ax)^2 + (By-Ay)^2} \quad (5.8)$$

and the angle α of the velocity vector with respect to the positive X-axis was:

$$\alpha = ARCTAN((By-Ay)/(Bx-Ax)) \quad (5.9)$$

In actual practice it was necessary to use a constant of proportionality (λ) between volumes Va and Vb due to the variance in the time interval occurring between successive traces. For the case of equal time intervals between

traces, λ was equal to 1.0. Given traces 1, 2, and 3 occuring at times t_1,t_2, and t_3 respectively, the equation relating Va to Vb was expressed as;

$$Va = \lambda Vb \tag{5.10}$$

where,

$$\lambda = \frac{t_2 - t_1}{t_3 - t_2} \tag{5.11}$$

C. THEORETICAL VELOCITIES

The exact solution for the component velocities of the laminar circular jet has been provided by H. Schlicting in reference 10 These expressions are:

$$u = \frac{\nu}{y} \gamma \frac{\{\xi - .25\xi^3\}}{\{1 + .25\xi^2\}^2} \tag{5.12}$$

$$v = \frac{\nu}{y} \frac{2\gamma^2}{\{1 + .25\xi^2\}^2} \tag{5.13}$$

where,

$$\xi = \gamma \frac{x}{y} \tag{5.14}$$

The component velocities u and v were in the +X and +Y directions respectively, ν is the kinematic viscosity, and γ is a constant of integration. Further, the momentum of the jet was constant and given by:

$$J_{jet} = 16/3 \ \pi \gamma^2 \nu^2 \rho \tag{5.15}$$

The momentum in the nozzle was given by the expression:

$$J_{nozzle} = 2\pi \int_0^R v^2 x \, dx \tag{5.16}$$

Substituting the expression for the velocity distribution in laminar pipe flow yielded:

$$J_{nozzle} = 4/3\ \bar{u}^2 v^2 R^2 \pi \rho \qquad (5.17)$$

where $\bar{u}$ was the mean nozzle velocity, ρ was the density of the fluid and R was the radius of the nozzle. Setting the equation 5.16 equal to equation 5.17 and solving for the constant of integration:

$$\gamma = \bar{u} \frac{R}{2\nu} \qquad (5.18)$$

Substituting equation 5.18 back into equations 5.12 and 5.13 yielded the component velocities as a function of x and y given the kinematic viscosity and mean nozzle velocity.

D. VELOCITY COMPUTATION PROGRAM

Appendix A contains the computer program used to determine fluid velocities. Given the coefficients of the fourth order approximation to four traces and the corresponding time intervals, this program computed the average fluid velocities of incremental volumes between traces 1 & 2 to traces 2 & 3 and, also, for incremental volumes of traces 2 & 3 to traces 3 & 4. Velocities were computed at intervals of 0.1 mm. The program also computed the theoretical velocity vectors over the same interval given the nozzle flow rate (mm^3/sec), nozzle diameter (mm), and fluid temperature(C). A second order polynomial approximation to the dynamic viscosity of the fluid (mineral spirits) as a function of temperature and a first order polynomial approximation to the density of the fluid as a function of temperature are included in the program. Theoretical velocities were computed at the midpoints of the displacement

vectors ($\overline{AB}$) calculated in the experimental data reduction portion of the program to facilitate comparison of the theoretical and experimentally determined velocities.

VI. RESULTS

Tables I through IV provide a comparison of the experimental and theoretical velocities for two vertical positions at two nozzle flow rates. In both cases, fluid velocity was a maximum in the vicinity of the jet centerline and decreased with increasing distance from the centerline. These figures also show the fluid velocities to decrease with increasing distance above the jet nozzle as expected.

A. ERROR ANALYSIS

Trace position measurements were based on the outside diameter of the nozzle which was included in each photograph. This diameter was measured to be 3.307 mm with an uncertainty of ±0.005 mm. Optical distortion resulting from the trace photographs was minimized through the use of high-quality optics, using the highest possible f stop (smallest lens aperature), and by centering the traces in the photographic frame. The overall accuracy of the digitized traces was estimated to be within 0.050 mm. The digitized traces were curve fitted using a third order polynomial. This fit provided an RMS error of less than 0.032 mm for all traces. The time interval between laser firings was measured on the strip chart recorder with an accuracy of ± 4 msec. The combined effect of these errors resulted in an experimental velocity error of 2.6%.

Nozzle flow rate measurements introduced the greatest error in the theoretical velocity calculations. The flow rate accuracy of ±0.08 mm^3/sec combined with the nozzle diameter error of ±.002 mm resulted in a mean nozzle velocity error of 9.0%.

VII. CONCLUSIONS

Velocities were computed using the pulsed nitrogen laser/photochromic dye flow visualization technique. The technique was validated by comparing experimentally determined velocity profiles with those calculated from the analytical solution. The difference between experimental and theoretical velocities were within the limits of experimental error except at the extreme values of x where it appeared the curve fit differed markedly from experimental values. This method for measuring velocity distributions appears to be both accurate and useful where flow geometries permit its application.

VIII. RECOMMENDATIONS

Observations in the development of the laminar jet application of the pulsed nitrogen laser/photochromic dye flow visualization technique have resulted in the following recommendations for further application of the technique:

1. Trace length is limited by laser beam penetration in the photochromic fluid. Further research into the selection of type and concentration of the photochromic dye and the hydrocarbon solvent could increase the trace length and thus permit greater application of the technique.

2. In the current work, the flow under investigation was removed from the front wall where the laser beam entered the test chamber. Since there was very little fluid flow in the region adjacent to this wall, the repeated laser firings caused saturation of the photochromic fluid which resulted in increased beam attenuation. This problem was alleviated during this work by operating the laser just long enough to obtain the desired traces. A 10-15 second waiting period between laser firing runs permitted transformation of the dye to the colorless state, reducing beam attenuation and enhancing trace length. Applications where there is flow along the laser beam entry boundary would not require this waiting period since exposed dye would be carried away from the location of the successive laser beam pulses.

3. Increased laser output would provide greater application of this flow visualization technique. The higher beam intensity could be used to improve trace length or to permit increased dye concentrations. The latter would increase dye persistence which would make the technique useful at higher fluid flow rates. The present work was severely restricted by flow rate due to the loss of trace

definition resulting from the greater trace elongation. The increased trace persistence afforded by higher dye concentrations would reduce this problem. Improving laser output to increase trace length would provide the obvious advantage of visualizing flow at a greater distance from the laser beam entry boundary and thus reduce wall effects on the flow under examination.

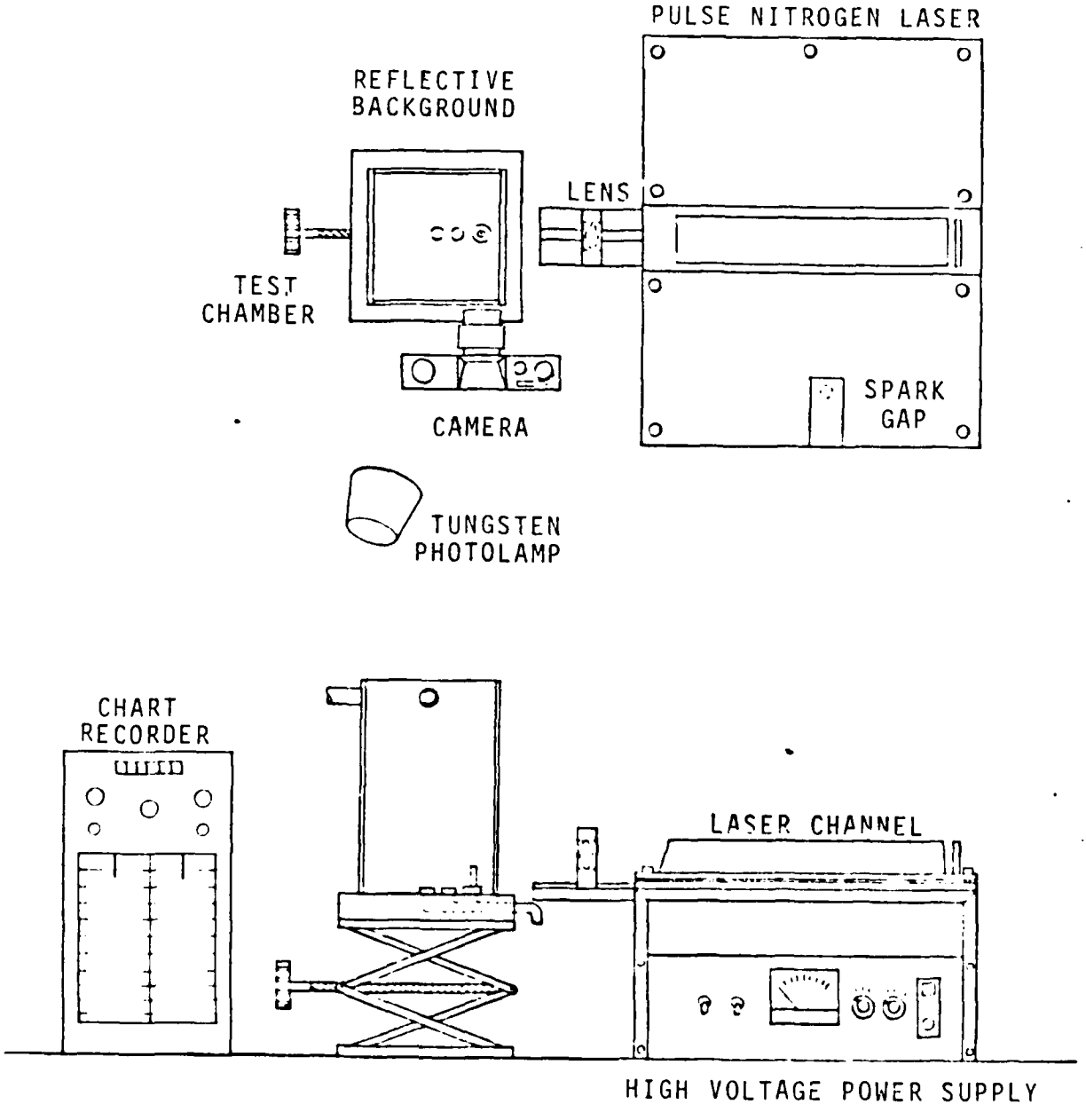

Figure 1 Experimental Apparatus

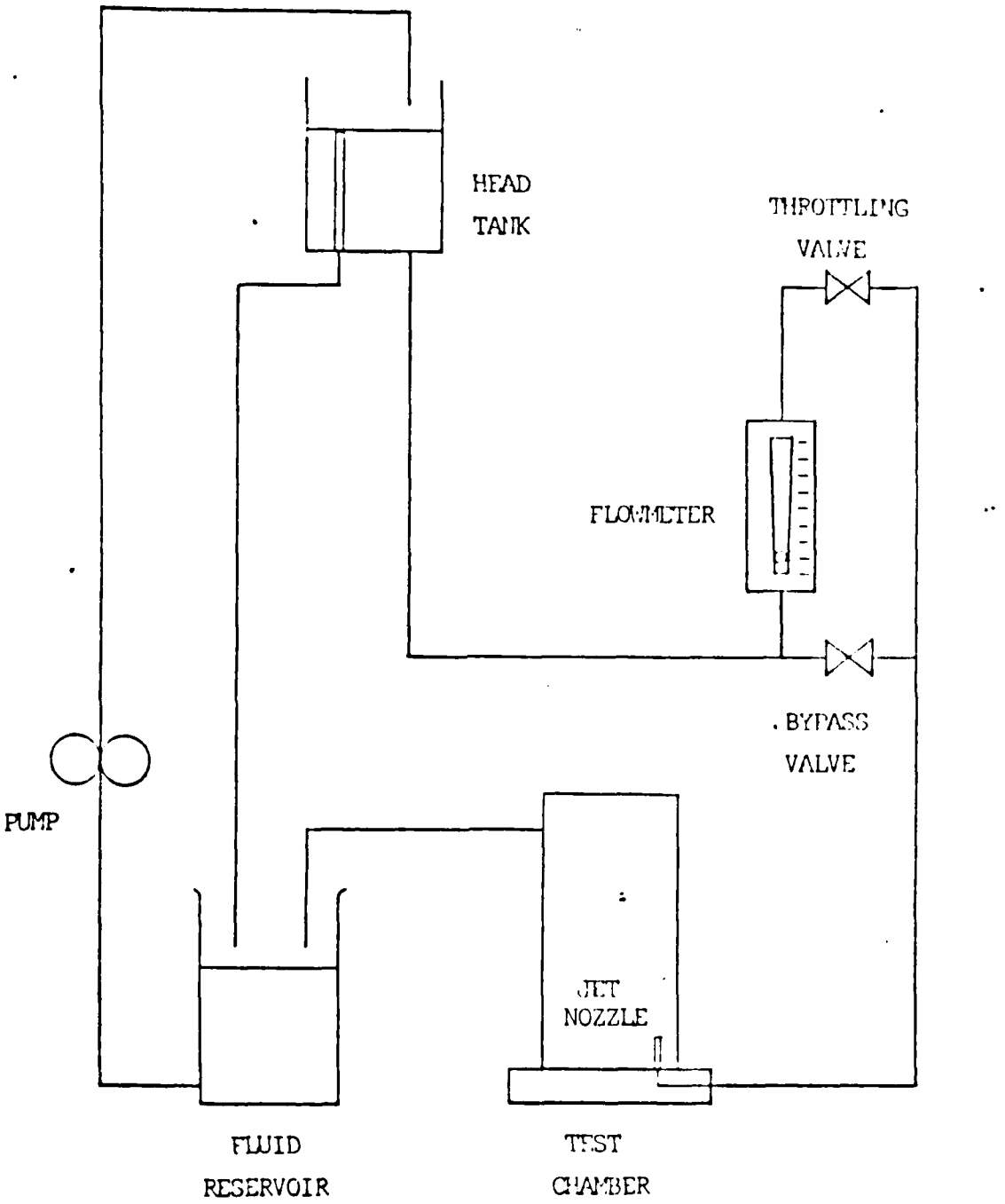

Figure 2 Flow System

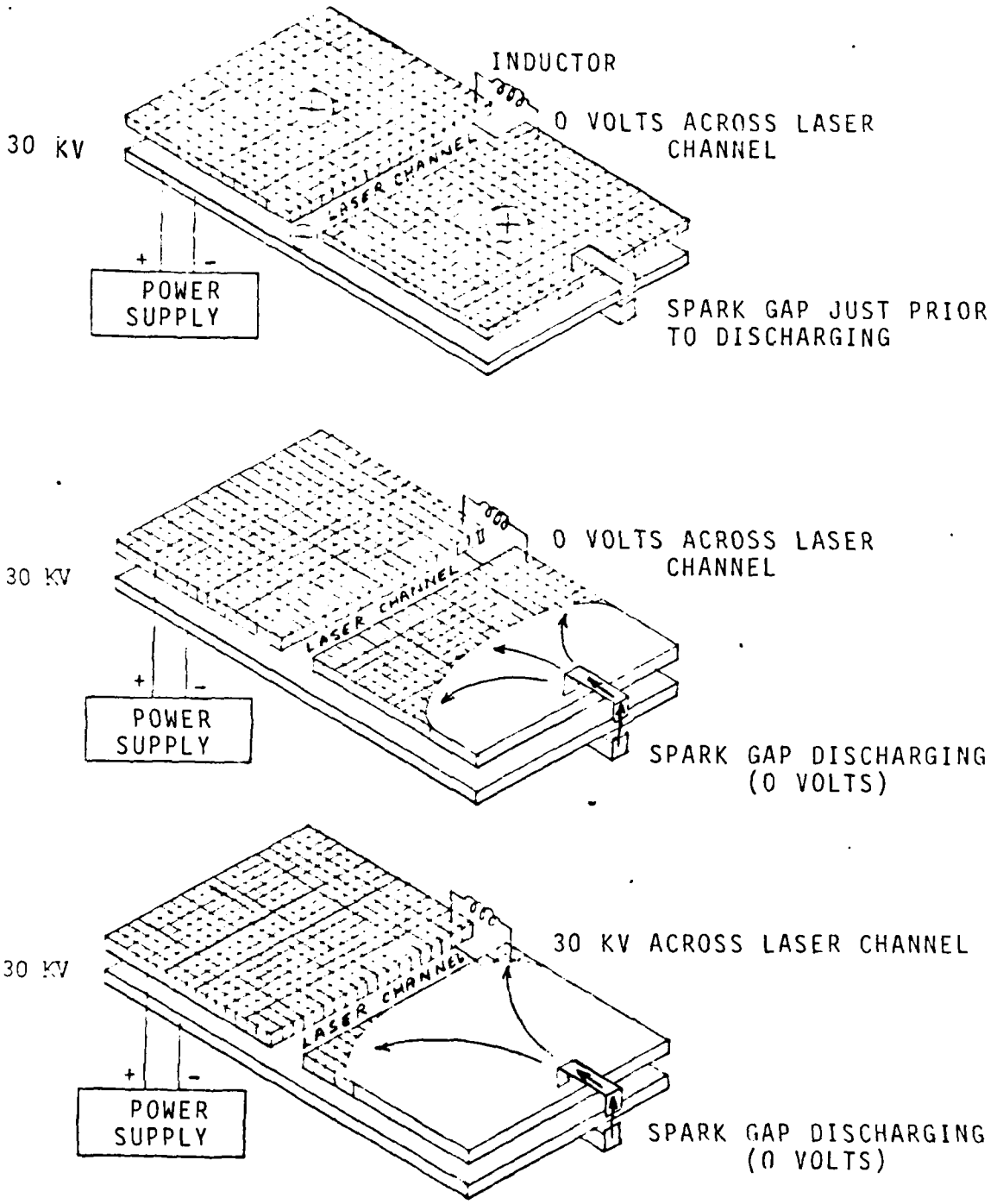

Figure 3 Nitrogen Laser Operation

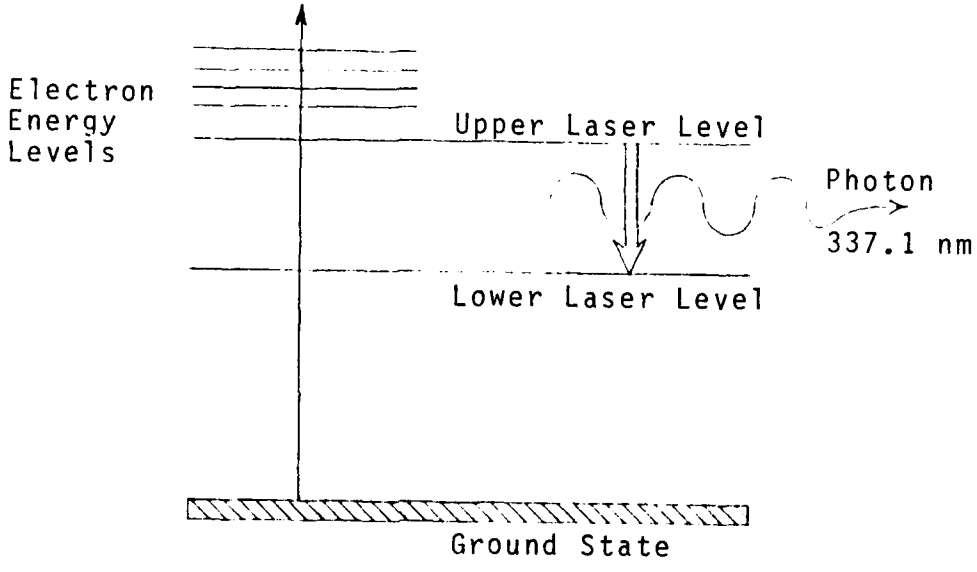

Figure 4 Nitrogen Electronic Energy Levels

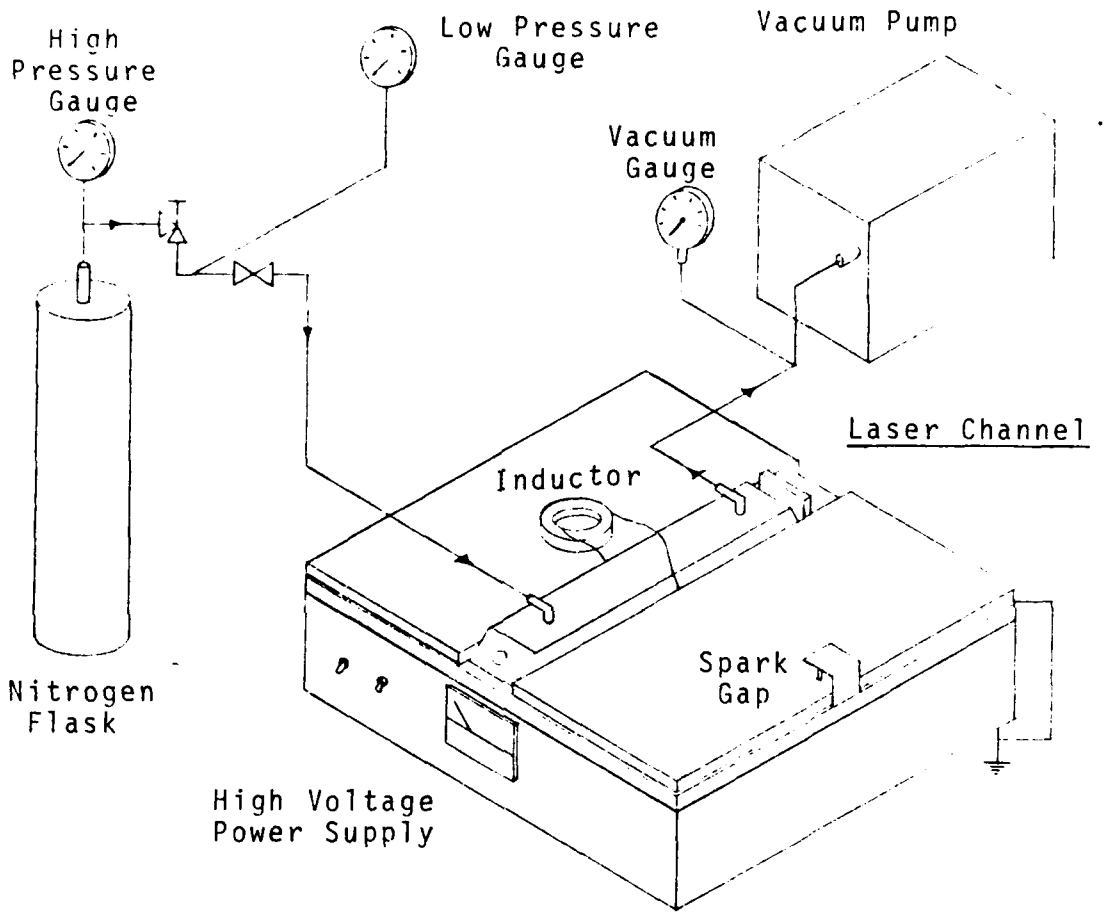

Figure 5 Pulsed Nitrogen Laser

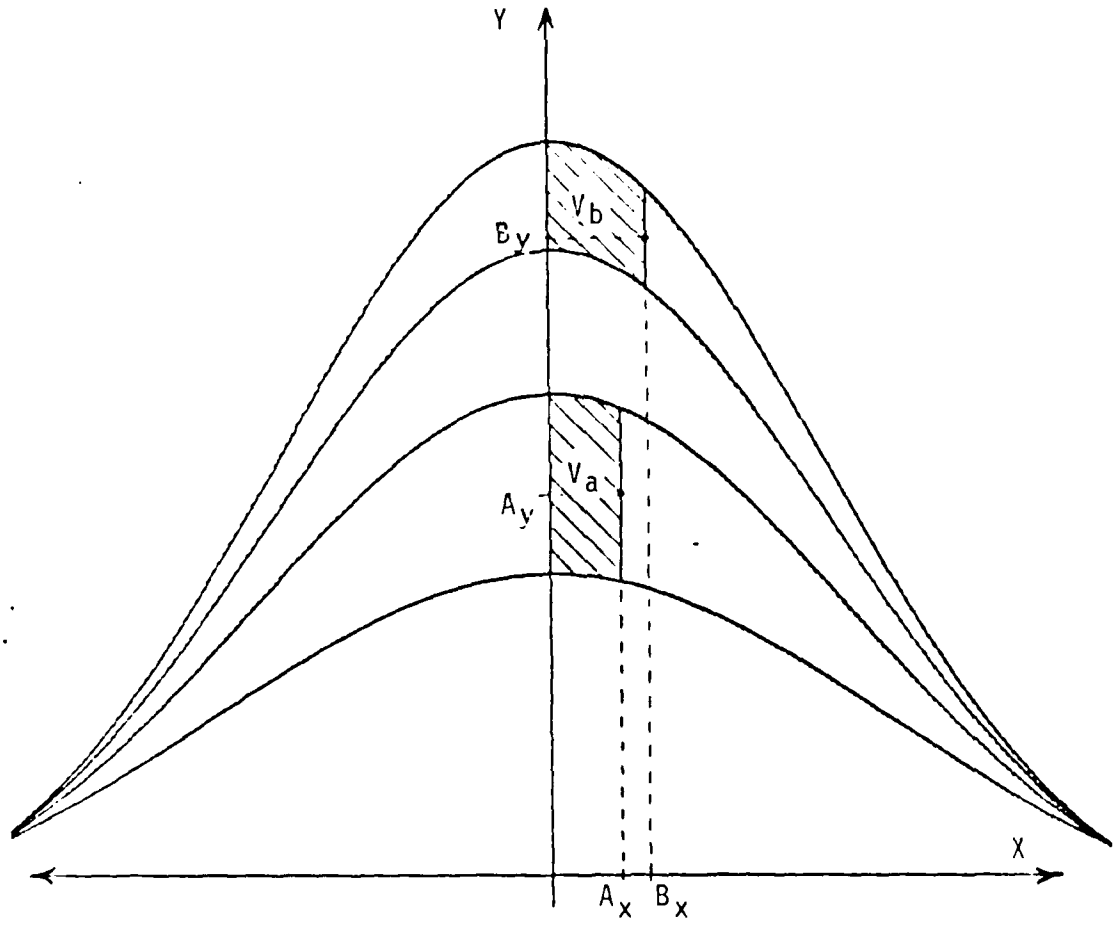

Figure 6 Velocity Calculation Technique

TABLE I

Laminar Jet Run 1

POSITION X	POSITION Y	TRACES 1-2-3 EXPERIMENTAL VELOCITY	TRACES 1-2-3 EXPERIMENTAL THETA	TRACES 1-2-3 THEORETICAL VELOCITY	TRACES 1-2-3 THEORETICAL THETA	TRACES 2-3-4 EXPERIMENTAL VELOCITY	TRACES 2-3-4 EXPERIMENTAL THETA	TRACES 2-3-4 THEORETI CAL VELOCITY	TRACES 2-3-4 THEORETI CAL THETA
-0.00	6.12	6.165	90.03	6.043	90.00	5.137	90.04	4.766	90.00
-0.10	6.12	6.146	90.19	6.036	90.48	5.135	90.51	4.764	90.39
-0.21	6.10	6.114	90.42	6.024	90.97	5.133	90.94	4.761	90.78
-0.31	6.08	6.069	90.61	6.008	91.45	5.133	91.33	4.758	91.17
-0.41	6.04	6.012	90.81	5.987	91.93	5.135	91.64	4.753	91.56
-0.52	5.99	5.942	90.99	5.959	92.42	5.138	91.91	4.747	91.95
-0.62	5.93	5.858	91.17	5.923	92.90	5.145	92.06	4.740	92.34
-0.72	5.85	5.761	91.32	5.878	93.39	5.153	92.18	4.730	92.72
-0.82	5.77	5.651	91.45	5.821	93.87	5.163	92.21	4.718	93.11
-0.92	5.67	5.526	91.55	5.752	94.34	5.174	92.17	4.703	93.50
-1.02	5.57	5.385	91.63	5.666	94.80	5.185	92.05	4.684	93.89
-1.12	5.46	5.227	91.68	5.563	95.25	5.200	91.81	4.659	94.28
-1.22	5.34	5.054	91.66	5.441	95.67	5.194	91.66	4.628	94.67
-1.32	5.22	4.859	91.61	5.296	96.06	5.165	91.55	4.589	95.06
-1.42	5.09	4.645	91.47	5.129	96.40	5.124	91.37	4.539	95.45
-1.52	4.96	4.399	91.33	4.937	96.68	5.057	91.19	4.476	95.82
-1.61	4.82	4.133	91.04	4.723	96.87	4.983	90.88	4.397	96.17
-1.71	4.68	3.827	90.71	4.484	96.94	4.876	90.58	4.298	96.49
0.00	6.12	6.165	89.97	6.043	90.00	5.137	89.96	4.766	90.00
0.10	6.11	6.171	89.81	6.047	89.52	5.137	89.45	4.768	89.60
0.21	6.08	6.164	89.65	6.046	89.04	5.135	88.91	4.769	89.21
0.31	6.05	6.146	89.52	6.040	88.55	5.128	88.36	4.770	88.81
0.41	6.00	6.118	89.46	6.030	88.07	5.113	87.81	4.770	88.41
0.51	5.94	6.077	89.39	6.012	87.59	5.091	87.28	4.770	88.00
0.61	5.86	6.026	89.38	5.987	87.10	5.056	86.75	4.768	87.59
0.71	5.78	5.963	89.41	5.953	86.62	5.006	86.24	4.765	87.18
0.81	5.69	5.891	89.50	5.907	86.14	4.939	85.74	4.760	86.76
0.91	5.58	5.804	89.63	5.847	85.67	4.851	85.24	4.752	86.34
1.01	5.47	5.659	89.48	5.768	85.18	4.742	84.80	4.740	85.91
1.11	5.34	5.460	89.18	5.665	84.69	4.611	84.39	4.721	85.48
1.21	5.20	5.233	88.92	5.538	84.24	4.456	84.01	4.695	85.05
1.32	5.05	4.976	88.71	5.384	83.82	4.282	83.72	4.657	84.62
1.42	4.89	4.695	88.59	5.199	83.47	4.083	83.46	4.603	84.21
1.52	4.73	4.380	88.53	4.983	83.21	3.866	83.30	4.531	83.82
1.61	4.57	4.038	88.60	4.736	83.07	3.656	83.41	4.434	83.48
1.71	4.41	3.683	88.94	4.463	83.10	3.449	83.77	4.307	83.21

Flowrate = 0.873 mm^3/s Temperature = 23.2C
Velocities in mm/s Theta in degrees
Positions in mm

TABLE II

Laminar Jet Run 2

POSITION X	POSITION Y	TRACES 1-2-3 EXPERIMENTAL VELOCITY	TRACES 1-2-3 EXPERIMENTAL THETA	TRACES 1-2-3 THEORETICAL VELOCITY	TRACES 1-2-3 THEORETICAL THETA	TRACES 2-3-4 EXPERIMENTAL VELOCITY	TRACES 2-3-4 EXPERIMENTAL THETA	TRACES 2-3-4 THEORETICAL VELOCITY	TRACES 2-3-4 THEORETICAL THETA
-0.00	7.00	5.459	90.04	5.377	90.00	4.127	90.05	4.559	90.00
-0.11	7.00	5.464	90.97	5.369	90.46	4.131	91.26	4.554	90.39
-0.22	6.99	5.450	91.94	5.353	90.92	4.128	92.52	4.544	90.78
-0.34	6.98	5.418	92.93	5.329	91.37	4.118	93.80	4.530	91.16
-0.45	6.96	5.367	93.94	5.296	91.82	4.101	95.09	4.511	91.55
-0.56	6.93	5.297	95.00	5.254	92.28	4.073	96.41	4.488	91.94
-0.67	6.89	5.206	96.11	5.204	92.72	4.035	97.77	4.461	92.32
-0.78	6.85	5.095	97.29	5.144	93.16	3.982	99.19	4.430	92.70
-0.90	6.80	4.962	98.56	5.074	93.60	3.914	100.71	4.394	93.08
-1.01	6.75	4.805	100.00	4.993	94.03	3.825	102.41	4.352	93.46
-1.12	6.69	4.623	101.66	4.902	94.45	3.711	104.36	4.306	93.84
-1.24	6.62	4.414	103.61	4.799	94.85	3.568	106.66	4.253	94.22
-1.35	6.55	4.175	105.99	4.684	95.24	3.390	109.52	4.195	94.60
-1.47	6.47	3.901	109.11	4.554	95.61	3.167	113.40	4.128	94.97
-1.59	6.38	3.591	113.41	4.409	95.96	2.893	119.07	4.052	95.35
-1.71	6.27	3.244	119.94	4.244	96.28	2.565	128.45	3.962	95.72
-1.85	6.15	2.881	130.95	4.050	96.56	2.238	146.19	3.852	96.10
-2.01	5.98	2.663	155.29	3.787	96.79	2.396	******	3.692	96.52
0.00	7.00	5.459	89.96	5.377	90.00	4.126	89.95	4.559	90.00
0.11	6.99	5.436	89.03	5.377	89.54	4.116	88.73	4.561	89.61
0.22	6.97	5.395	88.04	5.368	89.08	4.097	87.46	4.558	89.22
0.34	6.95	5.337	87.07	5.352	88.62	4.072	86.21	4.551	88.83
0.45	6.92	5.261	86.10	5.327	88.17	4.039	85.00	4.540	88.45
0.56	6.88	5.168	85.09	5.293	87.72	3.995	83.74	4.524	88.06
0.67	6.83	5.056	84.02	5.250	87.27	3.939	82.43	4.504	87.67
0.78	6.78	4.926	82.91	5.198	86.82	3.870	81.10	4.480	87.28
0.89	6.72	4.779	81.76	5.136	86.38	3.786	79.74	4.451	86.90
1.00	6.65	4.610	80.44	5.063	85.95	3.679	78.18	4.417	86.51
1.11	6.57	4.425	79.08	4.979	85.53	3.555	76.57	4.378	86.13
1.22	6.49	4.216	77.46	4.883	85.12	3.401	74.63	4.332	85.75
1.33	6.40	3.984	75.58	4.775	84.73	3.218	72.32	4.280	85.38
1.44	6.31	3.730	73.34	4.654	84.36	3.003	69.47	4.221	85.01
1.55	6.21	3.447	70.44	4.518	84.02	2.747	65.56	4.152	84.64
1.66	6.10	3.136	66.59	4.367	83.72	2.450	59.94	4.073	84.29
1.78	5.98	2.797	61.06	4.199	83.46	2.119	51.00	3.980	83.95
1.89	5.85	2.442	52.57	4.010	83.27	1.796	35.49	3.869	83.63

Flowrate = 0.873 mm^3/s Temperature = 23.2C
Velocities in mm/s Theta in degrees
Positions in mm

TABLE III

Laminar Jet Run 3

POSITION X	POSITION Y	TRACES 1-2-3 EXPERIMENTAL VELOCITY	TRACES 1-2-3 EXPERIMENTAL THETA	TRACES 1-2-3 THEORETICAL VELOCITY	TRACES 1-2-3 THEORETICAL THETA	TRACES 2-3-4 EXPERIMENTAL VELOCITY	TRACES 2-3-4 EXPERIMENTAL THETA	TRACES 2-3-4 THEORETICAL VELOCITY	TRACES 2-3-4 THEORETICAL THETA
-0.00	9.96	7.953	90.03	8.332	90.00	6.128	90.04	7.121	90.00
-0.11	9.95	7.918	90.72	8.333	90.32	5.958	90.88	7.135	90.27
-0.22	9.92	7.854	91.41	8.322	90.64	5.770	91.78	7.144	90.55
-0.33	9.88	7.760	92.13	8.297	90.96	5.562	92.75	7.145	90.83
-0.44	9.83	7.639	92.84	8.258	91.28	5.337	93.76	7.139	91.10
-0.55	9.76	7.490	93.56	8.205	91.60	5.095	94.83	7.126	91.38
-0.66	9.68	7.312	94.32	8.137	91.91	4.832	96.05	7.104	91.66
-0.77	9.59	7.107	95.10	8.051	92.22	4.550	97.38	7.073	91.94
-0.88	9.50	6.879	95.89	7.949	92.53	4.142	100.23	7.029	92.24
-0.99	9.39	6.619	96.75	7.828	92.83	3.575	105.68	6.968	92.57
-1.10	9.27	6.331	97.69	7.688	93.12	2.861	116.32	6.885	92.92
-1.21	9.14	5.974	99.07	7.522	93.41	2.099	144.36	6.767	93.32
-1.36	8.92	5.049	106.28	7.259	93.79	2.955	******	6.564	93.83
-1.57	8.59	3.612	129.93	6.840	94.23	49.174	******	1.910	61.47
0.00	9.96	7.954	89.97	8.332	90.00	6.131	89.96	7.120	90.00
0.11	9.97	7.957	89.29	8.318	89.68	6.281	89.17	7.100	89.73
0.22	9.96	7.931	88.60	8.293	89.36	6.410	88.40	7.073	89.46
0.33	9.93	7.873	87.90	8.255	89.04	6.519	87.66	7.041	89.19
0.44	9.89	7.785	87.21	8.204	88.73	6.605	86.96	7.003	88.92
0.55	9.84	7.667	86.53	8.142	88.42	6.669	86.31	6.960	88.65
0.66	9.78	7.517	85.80	8.065	88.11	6.707	85.65	6.912	88.39
0.77	9.70	7.332	85.02	7.975	87.80	6.716	84.97	6.858	88.12
0.88	9.61	7.118	84.24	7.870	87.50	6.698	84.34	6.798	87.86
0.99	9.51	6.868	83.38	7.749	87.20	6.647	83.68	6.732	87.60
1.10	9.39	6.578	82.41	7.611	86.91	6.557	82.96	6.658	87.34
1.21	9.27	6.247	81.29	7.454	86.63	6.425	82.17	6.576	87.09
1.32	9.13	5.871	79.96	7.278	86.36	6.244	81.28	6.485	86.83
1.43	8.97	5.442	78.28	7.079	86.10	6.004	80.20	6.383	86.58
1.54	8.81	4.948	76.02	6.855	85.87	5.687	78.79	6.267	86.34
1.65	8.62	4.379	72.75	6.604	85.67	5.276	76.84	6.134	86.10
1.77	8.42	3.723	67.52	6.321	85.51	4.738	73.87	5.980	85.87
1.89	8.20	2.960	57.38	5.995	85.41	4.000	68.36	5.794	85.66

Flowrate = 1.30 mm^3/s Temperature = 24.3 C
Velocities in mm/s Theta in degrees
Positions in mm

TABLE IV

Laminar Jet Run 4

POSITION X	POSITION Y	TRACES 1-2-3 EXPERIMENTAL VELOCITY	TRACES 1-2-3 EXPERIMENTAL THETA	TRACES 1-2-3 THEORETICAL VELOCITY	TRACES 1-2-3 THEORETICAL THETA	TRACES 2-3-4 EXPERIMENTAL VELOCITY	TRACES 2-3-4 EXPERIMENTAL THETA	TRACES 2-3-4 THEORETICAL VELOCITY	TRACES 2-3-4 THEORETICAL THETA
-0.00	11.33	6.084	90.04	7.328	90.00	5.689	90.04	6.488	90.00
-0.10	11.33	6.069	90.11	7.322	90.26	5.693	90.20	6.484	90.23
-0.20	11.32	6.055	90.19	7.307	90.51	5.699	90.36	6.475	90.46
-0.30	11.30	6.041	90.27	7.285	90.77	5.708	90.52	6.459	90.69
-0.40	11.28	6.028	90.31	7.254	91.02	5.720	90.64	6.438	90.91
-0.50	11.25	6.016	90.34	7.214	91.27	5.732	90.80	6.411	91.14
-0.60	11.22	6.004	90.34	7.166	91.52	5.745	90.92	6.378	91.36
-0.70	11.17	5.994	90.31	7.109	91.76	5.754	91.08	6.338	91.59
-0.80	11.12	5.982	90.27	7.044	92.01	5.759	91.24	6.293	91.81
-0.90	11.07	5.972	90.15	6.970	92.25	5.757	91.40	6.243	92.03
-1.00	11.00	5.961	90.00	6.888	92.48	5.745	91.56	6.186	92.25
-1.10	10.94	5.944	89.85	6.796	92.71	5.716	91.77	6.123	92.47
-1.20	10.86	5.927	89.61	6.696	92.93	5.669	91.99	6.054	92.69
-1.29	10.78	5.906	89.34	6.588	93.15	5.597	92.26	5.978	92.90
-1.39	10.70	5.877	89.02	6.471	93.35	5.491	92.59	5.896	93.12
-1.48	10.61	5.840	88.66	6.345	93.55	5.347	93.01	5.807	93.33
-1.59	10.51	5.727	88.79	6.201	93.75	5.150	93.57	5.709	93.53
-1.69	10.41	5.557	89.17	6.042	93.95	4.889	94.33	5.603	93.73
0.00	11.33	6.083	89.96	7.328	90.00	5.689	89.96	6.488	90.00
0.10	11.32	6.097	89.89	7.325	89.74	5.689	89.80	6.485	89.77
0.20	11.31	6.110	89.77	7.315	89.49	5.690	89.60	6.477	89.54
0.30	11.29	6.121	89.70	7.295	89.23	5.693	89.39	6.463	89.31
0.41	11.26	6.129	89.59	7.268	88.98	5.696	89.19	6.444	89.08
0.51	11.22	6.133	89.51	7.231	88.72	5.698	88.99	6.418	88.85
0.61	11.18	6.133	89.47	7.186	88.47	5.694	88.75	6.387	88.63
0.71	11.13	6.125	89.40	7.132	88.22	5.687	88.55	6.351	88.40
0.81	11.07	6.111	89.40	7.069	87.97	5.669	88.30	6.309	88.17
0.91	11.00	6.087	89.40	6.997	87.73	5.638	88.04	6.261	87.95
1.01	10.93	6.049	89.39	6.916	87.49	5.595	87.82	6.209	87.72
1.11	10.85	5.999	89.42	6.825	87.25	5.530	87.55	6.150	87.50
1.21	10.76	5.929	89.46	6.724	87.02	5.445	87.30	6.086	87.28
1.31	10.67	5.846	89.57	6.614	86.80	5.332	87.03	6.016	87.06
1.40	10.57	5.735	89.64	6.493	86.58	5.186	86.72	5.940	86.84
1.50	10.47	5.604	89.79	6.363	86.38	5.010	86.42	5.857	86.63
1.60	10.36	5.443	89.96	6.222	86.18	4.791	86.07	5.766	86.42
1.70	10.24	5.246	90.13	6.071	86.00	4.533	85.69	5.668	86.22

Flowrate = 1.30 mm^3/s Temperature = 24.3 C
Velocities in mm/s Theta in degrees
Positions in mm

APPENDIX A

JET VELOCITY COMPUTER PROGRAM

```
C This program computes experimental and theoretical jet velocities given
C the coefficients of the 4th order polynomial curve fit for each of four
C laser traces and the time each trace occurs.  Velocities are computed
C in the jet from x=-1.80 mm to x=1.80 mm.  Velocities are determined
C for traces 1&2 to 2&3 and also for traces 2&3 to 3&4.  Given the flow-
C rate, nozzle diameter, and temperature of the fluid (mineral spirits),
C this program computes the theoretical velocities using Schlicting's
C similarity solution at points corresponding to those of the experimen-
C tal velocities.
      IMPLICIT REAL*8 (A-H,O-Z)
      REAL KVISC
      DIMENSION A(4),B(4),C(4),D(4),E(4),DA(4),DB(4),DC(4),DD(4),DE(4),
     XAY(3),V1(2),V2(3),T(4),BY(3),THETA(3),DT(3),VEL(3),X(2),Y(2),
     XXI(2),U(2),V(2),THVEL(2),THETAT(2)
C
      PI=3.141592654D0
      T(1)=0.0
C
C Read flowrate(mm³/s),nozzle diameter(mm), and temperature(C)
C
      READ (7,*) Q,DIA,TEMP
      WRITE (6,101) Q,DIA,TEMP
101   FORMAT('1','Q=',F5.3,3X,'DIA=',F6.4,3X,'TEMP=',F4.1//)
      READ (7,*)'T(2),T(3),T(4)
C
      DO 10 I=1,4
         READ (7,*) A(I),B(I),C(I),D(I),E(I)
10    CONTINUE
C
C Determine the average time between traces 1&2 and 2&3 {DT(1)} and
C between traces 2&3 and 3&4{DT(2)}
C
      DT(1)=(T(3)+T(2))/2.-T(2)/2.
      DT(2)=(T(4)+T(3))/2.-(T(3)+T(2))/2.
C
C UM = mean nozzle velocity (mm/s)
C DYVISC = dynamic viscosity (kg/m-s)
C DENS = density of mineral spirits (kg/m³)
C KVISC = kinematic viscosity (mm²/s)
C GAMMA = constant of integration
```

```
C
      UM=4.*Q/(PI*DIA**2)*16.666667
      DYVISC=(2.05517374-3.4651131E-2*TEMP+2.9038264E-4*TEMP**2-
     X        1.0306034E-6*TEMP**3)*1.E-3
      DENS=(0.77075806-0.72580645E-3*TEMP)*1.E3
      KVISC=DYVISC/DENS*1.E6
      GAM=UM*DIA/4./KVISC
      WRITE(6,510)DYVISC,DENS,KVISC,GAM
510   FORMAT(2X,'DYVISC,DENS,KVISC,GAM'/4(F12.8,3X)//)
C
      WRITE (6,1000)
C
C Compute differences between successive trace coefficients
C
      DO 20 I=1,3
         DA(I)=A(I+1)-A(I)
         DB(I)=B(I+1)-B(I)
         DC(I)=C(I+1)-C(I)
         DD(I)=D(I+1)-D(I)
         DE(I)=E(I+1)-E(I)
20    CONTINUE
C
C Initialize Ax and Bx
C
      M=1
25    AX=0.D0
      BX=0.D0
C
C Increment x from 0.0 to 1.8 mm
C
30    DO 500 J=1,18
C
         DO 400 I=1,2
C
C Determine Ay for given Ax value
C
         AY(I)=(DA(I)+DB(I)*AX+DC(I)*AX**2+DD(I)*AX**3+DE(I)*AX**4)/2.
     X          + A(I)+B(I)*AX+C(I)*AX**2+D(I)*AX**3+E(I)*AX**4
C
C Determine Va for given Ax value
C
         V1(I)=DA(I)/2.*AX**2+DB(I)/3.*AX**3+DC(I)/4.*AX**4+DD(I)/5.
     X          *AX**5+DE(I)/6.*AX**6
C
C Solve for Bx where Vb = Va
C
```

```
          DO 100 K=1,2000
C
             V2(I)=(DA(I+1)/2.*BX**2+DB(I+1)/3.*BX**3+DC(I+1)/4.*BX**4
     X              + DD(I+1)/5.*BX**5+DE(I+1)/6.*BX**6)*(T(I+1)-T(I))/
     X              (T(I+2)-T(I+1))
C
             IF(V2(I).GT.V1(I)) GO TO 150
             BX=(DABS(BX)+0.001)*(-1.)**M
100       CONTINUE
C
C Solve for By at Bx
C
150       BY(I)=(DA(I+1)+DB(I+1)*BX+DC(I+1)*BX**2+DD(I+1)*BX**3+DE(I+1)*
     X          BX**4)/2.+A(I+1)+B(I+1)*BX+C(I+1)*BX**2+D(I+1)*BX**3
     X          + E(I+1)*BX**4
C
C Determine magnitude of velocity vector
C
          VEL(I)=DSQRT((BX-AX)**2+(BY(I)-AY(I))**2)/DT(I)
C
C Determine angle of velocity vector
C
          IF(AX.EQ.BX) GO TO 160
          RISE=BY(I)-AY(I)
          RUN=BX-AX
          THETA(I)=DATAN2(RISE,RUN)*360./(2.*PI)
          GO TO 180
160       THETA(I)=90.
C
C Determine midpoint of displacement vecotr and solve for theoretical
C velocity at this point.  U is the x-component of velocity and V is
C the y-component of velocity
C
180    X(I)=(AX+BX)/2.
       Y(I)=(AY(I)+BY(I))/2.
       XI(I)=GAM*X(I)/Y(I)
       V(I)=KVISC/Y(I)*2.*GAM**2/(1.+0.25*XI(I)**2)**2
       U(I)=KVISC/Y(I)*GAM*(XI(I)-0.25*XI(I)**3)/(1.+0.25*XI(I)**2)**2
       THVEL(I)=DSQRT(U(I)**2+V(I)**2)
       THETAT(I)=DATAN2(V(I),U(I))*360./(2.*PI)
400    CONTINUE
C
C Print: X and Y positions
C        Experimental and theoretical velocities for traces 1-2-3
CC       Experimental and theoretical velocities for traces 2-3-4
C
```

```
      WRITE (6,1200)X(1),Y(1),VEL(1),THETA(1),THVEL(1),THETAT(1),
     XVEL(2),THETA(2),THVEL(2),THETAT(2)
C
C Increment Ax and continue Do Loop
C
      AX=(DABS(AX)+0.1)*(-1.)**M
500   CONTINUE
C
C When negative x-values have been completed, set M=2 and compute
C velocities for positive x-values
C
      IF(M.EQ.2) GO TO 600
      M=2
      GO TO 25
600   CONTINUE
C
1000  FORMAT(24X,'TRACES 1-2-3',22X,'TRACES 2-3-4'//3X,'POSITION',
     X4X,'EXPERIMENTAL',6X,'THEORETICAL',5X,'EXPERIMENTAL',6X,'THEORETI
     XCAL'/4X,'X',5X,'Y',3X,4('VELOCITY',1X,'THETA',3X)/)
C
1200  FORMAT(2X,F5.2,1X,F5.2,1X,2(F6.3,2X,F6.2,3X,F6.3,2X,F6.2,3X))
C
      STOP
      END
```

LIST OF REFERENCES

1. Pellin, A. F., An Experimental Technique for the Study of Velocity Profiles in a Growing Droplet Using a Pulsed Nitrogen Laser, M.S. Thesis, Naval Postgraduate School, 1982.

2. Miller, S., Photochemical Reaction for the Study of Velocity Patterns and Profiles, B.A.Sc. Thesis, University of Toronto, 1962.

3. Goldfish, L. H., Koutsky, J. A., and Adler, R. J., "Tracer Introduction by Flash Photolysis", Chemical Engineering Science, Vol. 20, 1965.

4. Popovich, A. T., and Hummel, R. L., "A New Method for Non-Disturbing Turbulent Flow Measurements Very Close to a Wall", Chemical Engineering Science, 21, 1967.

5. Humphrey, J. A. C., "Light Induced Disturbances in Photochromic Flow Visualization", Canadian Journal of Chemical Engineering, Vol. 52, Feb 1974.

6. Humphrey, J., Hummel, R., and Smith, J., "Experimental Study of the Internal Fluid Dynamics of Forming Drops", Canadian Journal of Chemical Engineering, Vol. 52, August 1972.

7. Culbreth, W., Johnson, G., and Marschall, E., "Heat Transfer and Hydrodynamics During Drop Formation and Release in a Liquid Heat Exchanger", AIChE Symposium Series, 1981.

8. Strong, C. L., "The Amateur Scientist", Scientific American, June 1974.

9. American National Standard for the Safe Use of Lasers, American National Standards Institute, 1980.

10. Schlichting, H., Boundary-Layer Theory, pp. 230-234, McGraw-Hill, 1979.

INITIAL DISTRIBUTION LIST

No.		Copies
1.	Defense Technical Information Center Cameron Station Alexandria, Virginia 22314	2
2.	Library, Code 0142 Naval Postgraduate School Monterey, California 93943	2
3.	Department Chairman, Code 69 Department of Mechanical Engineering Naval Postgraduate School Monterey, California 93943	1
4.	Professor W. G. Culbreth, Code 69Cb Department of Mechanical Engineering Naval Postgraduate School Monterey, California 93943	5
5.	Lieutenant Commander David T. Armstrong 3136 Rossmoor Pkwy #7 Walnut Creek, California 94595	5

END

FILMED

4-85

DTIC